Metallomics

Accepted Manuscript

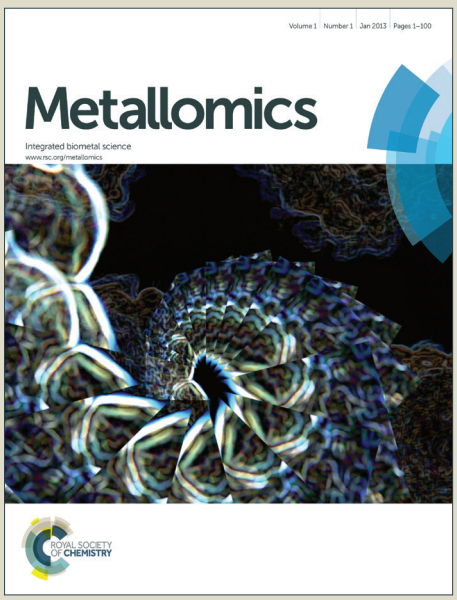

ROYAL SOCIETY OF CHEMISTRY

www.rsc.org/metallomics

Evaluation of Photo-reactive Siderophore Producing Bacteria Before, During and After a Bloom of the Dinoflagellate *Lingulodinium polyedrum*.

Kyoko Yarimizu[†], Geraldine Polido[†], Astrid Gärdes[|†], Melissa L. Carter[‡], Mary Hilbern[‡], and Carl J. Carrano*[†]

[†]Department of Chemistry & Biochemistry, San Diego State University, San Diego, CA 92182

and

[‡]Scripps Institution of Oceanography, San Diego, CA 92093

[|]Current Address: Leibniz Center for Tropical Marine Ecology (ZMT), Fahrenheitsstr. 6, 28359 Bremen, Germany.

Abstract

Evidence is increasing for a mutualistic relationship between phytoplankton and heterotrophic marine bacteria. It has been proposed that bacteria producing photoactive iron binding compounds known as siderophores could play an important role in such mutualistic associations by producing bioavailable iron utilizable by phytoplankton and in exchange receive autotrophically derived DOM. In order to understand the potential photoactive siderophores might be playing in bacterial-algal mutualism or marine biogeochemistry in general, it is important to be able to detect and quantify their presence in various environments. One approach to accomplish that end is to make use of high sensitivity genomics technology (qPCR) to search for siderophore biosynthesis genes related to the production of photoactive siderophores. In this way one can access their "biochemical potential" and utilize this information as a proxy for the presence of these siderophores in the marine environment.

In this report we studied the correlation between the presence of bacteria producing one of four photoactive siderophores relative to total bacterial and dinoflagellate numbers from surface water at the Scripps Pier before, during, and after fall bloom of the dinoflagellate *Lingulodinium polyedrum*. We believe these findings will aid us in gauging the importance of photoactive siderophores in the marine environment and in harmful algal bloom dynamics in particular.

Introduction

Algal blooms are ubiquitous phenomena that have been increasingly observed in the coastal and upwelling parts of the world's oceans.[1,2] Even in the absence of toxin production these events often alter the chemical and ecological environment by changing nutrient distribution and the biodiversity of marine ecosystems.[3] Consequently these blooms often have immediate acute effects on marine populations and their impact on public health and local economies is large and has been increasing.[1,4] Although many physical and biological factors influence bloom dynamics, emerging evidence suggests that bacterial-algal interactions may be contributing to their development and sustenance.[5-9] Indeed, some bacterial associates of harmful algal species are clearly important to the physiological welfare of algal cells as evidenced by the fact that many species such as the dinoflagellate *Gymnodinium catenatum* cannot be grown axenically indicating an obligatory requirement(s) that is supplied by bacteria.[10,11] Thus, bacterial-algal interactions are likely to be strongly influenced by the supply of available nutrients. While nitrogen, phosphorous and vitamins have most often been considered in this context, a broad hypothesis that links these bacterial 'symbionts' to the growth of dinoflagellates, diatoms and coccolithophores is in their possible control of the supply of iron.

Iron is an essential nutrient for photosynthesis and respiration in all microorganisms, including phytoplankton and marine bacteria. Despite the fact that iron is the fourth most abundant element on the earth, iron levels in oceanic surface water are extremely low.[12-14] Consequently, iron acquisition from the environment is a significant challenge for microorganisms. The production of organic ligands to complex, solubilize and transport ferric ions is one common strategy used by bacteria to facilitate uptake of iron.[15] These ligands, known as siderophores, which come in a wide variety of structures, have also been identified as the iron-

binding ligands produced by marine bacteria.[16,17] One of the characteristic features that seem to distinguish marine from terrestrial siderophores is the near ubiquitous presence of α-hydroxy acid groups in the former which renders their ferric complexes photolabile through a photochemical process such as that shown below, where sid* is the siderophore derived photoproduct:[18-20]

$$\text{Fe(III)-siderophore} + h\nu \rightarrow \text{Fe(II)} + \text{sid*} + CO_2 + 2H^+$$

In contrast to marine bacteria, phytoplankton are not known to produce ligands like siderophores or to directly take up bacterial derived ferric-siderophore complexes. However evidence is increasing for a mutualistic relationship between phytoplankton and some marine bacteria and we hypothesize that photoactive siderophores could play an important role in such mutualistic associations through the generation of bioavailable free Fe(II) and/or Fe(III).[21]

To understand the potential photoactive siderophores might be playing in bacterial-algal mutualism or marine biogeochemistry in general it is important to be able to detect and quantify their presence in various environments. Unfortunately it has been a challenge for researchers to directly measure the quantity of photoactive siderophores due to their low concentration in the marine environment, and their rapid degradation by photochemical reactions. An alternative approach is to make use of high sensitivity genomics technology (qPCR) to search for siderophore biosynthesis genes related to the production of photoactive siderophores. In this way one can access their "biochemical potential" and utilize this information as a proxy for the presence of these siderophores in the marine environment.[22] Here we quantify siderophore biosynthetic genes to act as surrogates for the presence of three photoactive siderophores (petrobactin, aerobactin, and vibrioferrin) in sea surface water at the Scripps Pier (La Jolla, CA)

before, during, and after a bloom of the dinoflagellate *Lingulodinium Polyedrum* (*L. polyedrum*) during September and October of 2011.

Methods

The sampling site: The Scripps Institution of Oceanography (SIO) pier (La Jolla, CA; 32°53′N, 117°15′W) is a long-term coastal monitoring site in the Southern California Bight. The sampling site is beyond the surf zone and has a bottom depth of 7 m on average with a spring tidal range of 2 m. The site is well known to experience cycles in phytoplankton abundance, such as *Synechococcus sp.*[23] as well as larger diatoms and dinoflagellates like *L. polyedrum*, including intense blooms such as that during October 2011.

Chlorophyll and phytoplankton cell counts: Sea surface water samples were collected weekly at Scripps Pier as part of the Southern California Coastal Ocean Observing Harmful Algal Bloom Monitoring Program (http://www.sccoos.org/data/chlorophyll/index.php). Chlorophyll (Chl *a*) values were obtained using standard chlorophyll extraction and analysis procedures outlined by Venrick and Haywayd, in which seawater was filtered through a GF/F filter (approximately 0.7μm pore size) and then extracted in 90% acetone for 24 hours before reading on a calibrated fluorometer.[24] Abundance of phytoplankton groups (diatoms, dinoflagellates) and specific species were determined from settling 10 mL of seawater preserved with 4% formaldehyde.[25,26] Cells were identified and counted to lowest taxonomic level with a phase-contrast, inverted light microscope at 200X. The total volume of material counted was 2.5 mL with a detection limit of 400 cells/L.

Quantification of biosynthesis genes by real time qPCR: Sea surface water was collected from the Scripps Pier at seven different time points from 09/23/11-10/30/11. The collected sea surface water was immediately filtered through double connected membranes (0.8μm and 0.2μm pore

size) to separate particle-associated bacteria from free-living bacteria. DNA was extracted chemically from both of the bacteria containing membranes using the XS buffer method.[27,28]

The preparation of the degenerate primers for the genes encoding for photoactive siderophore biosynthesis i.e. *asbE* for petrobactin, *iucC* for aerobactin, and *pvsB* for vibrioferrin was previously described.[22] As it proved impossible to make a single set of degenerate primers that could adequately quantitate the *pvsB* gene for both *Marinobacter* produced vibrioferrin, and non-*Marinobacter* produced vibrioferrin, we developed two separate primers designated as pvsB for the former and *vibXII* for the latter. These primers were used in conjunction with qPCR to quantify the presence of biosynthetic genes for the three photoactive siderophores in the samples. Additionally, universal bacterial *16S* primers were utilized for a Taq-Man assay to estimate total bacterial abundance.[29,30] Standards used for quantification were genomic DNA prepared from *Marinobacter algicola DG893* (BLAST code AY258110), *Vibrio splendidus* (BLAST code A4353085), *Marinobacter aquaeolei* (BLAST code NC_008740) and *Vibrio fisherii* MJ11 (BLAST code NC_011184). Each qPCR sample contained 12.5 μL SYBR Green PCR Master Mix (Bio-Rad, P/N 1725120), 1 μM each primer, 2 μL template DNA and water to a final 25 μL volume while each Taq-Man sample contained 2x Super Mix, (Bio-Rad, P/N 170-8860), 0.9 μM each primer, 2 μL template DNA, 0.25 μM of TAMRA probe (Applied Biosystems, P/N 450025), and water to a final 25 μL volume. All reactions were performed in 96 well q-PCR plates. Gene copy numbers of each siderophore biosynthetic gene were determined for both the particle-associated (0.8 μm filter) and free-living (0.2 μm filter) bacterial fractions by qPCR using standard curves. All qPCR were run using an ICycler IQ-5 thermocycler equipped with a multicolor detection system and analyzed by the Bio-Rad IQ-5 Software 2.0. The qPCR temperature program consisted of an initial incubation at 95 ˚C for 5 min, followed by 45 cycles

of 95 ˚C for 10 s and 60 ˚C for 1 min. The Taq-Man temperature program consisted of an initial incubation at 93 ˚C for 10 min, followed by 45 cycles of 95 ˚C for 20 s and 62 ˚C for 1 min. The qPCR and Taq-Man assays of the sample DNA extracts were performed in triplicate and duplicate, respectively. Samples that did not exhibit any background fluorescence including primer-dimer formation were assumed to be inhibited for qPCR, and thus the DNA was further purified using QIAamp DNA Stool Mini Kit (Qiagen, P/N 51504).

Calculations: Relative abundance of the genes of interest were determined by comparison to the total bacterial *16S* rRNA gene pool. One genome was assumed to be the average size of 3.0 MB for the particle associated bacteria and 1.6 MB for the free living component.[31] The number of 16S gene per genome was assumed to be 1.8 for both the particle associated bacteria and the free living bacteria.[32]

Phylogenetic analysis of products amplified by qPCR: Representative field DNA samples amplified by qPCR were selected from beginning, during and end of the bloom time points. The amplified qPCR products were inserted in pGEM-T Easy vector System I (Promega) and transformed in host organism, *E. Coli* competent cells. The inserted DNA was sequenced by Microchemical Core Facility (SDSU). The protein sequence of the insert was searched by BLAST. The clone library was constructed from the protein sequences. Using Geneious R6 program, phylogenetic affiliation was established by alignment of the translated clone sequences against previously used known sequences.[33] Tree construction was based on amino acid substitution using PHYML with rate optimization as implemented in Geneious R6.[34]

Results

Bloom Dynamics. As can be seen in figure 1A dinoflagellate abundance, mainly *L. polyedrum*, increased from less than 50,000 cells/L in the beginning of September to a peak of ca.

150,000,000 cells/L on October 3rd and then declined to below detection levels by the end of October. Diatoms showed a reverse trend in that their abundance was high before and after the *L. polyedrum* bloom and at a minimum when dinoflagellate abundance peaked. The concentration of chlorophyll, which represents an estimate of algal biomass, tracked dinoflagellate abundance. Phaeophytin, which is a pigment derived from the degradation of chlorophyll, was relatively low compared to the chlorophyll yield (figure 1B).

q-PCR. Bacterial numbers (free living/particle-associated/total) were determined by Taq-Man PCR assay based on 16S gene copy numbers (Tables S1 and S2 supplementary material). Free living bacterial numbers peaked on Oct. 2nd and then declined throughout the remaining sampling period. Particle-associated bacterial numbers on the other hand showed maxima on Oct 2nd (prebloom), Oct. 9th (beginning of bloom decline), and Oct. 30th (post bloom) with a minimum on Oct. 5th at the bloom maximum. It is notable that particle-associated bacteria constituted the majority of the total bacterial numbers at all time points (see figs. 2-4). However, the relative fraction of the free living component was largest at the early time points (prebloom) and declined to a very small faction post bloom.

Gene copy numbers for both free-living and particle-associated bacteria producing the photoactive siderophores vibrioferrin (primers pvsB and vibXII) and petrobactin (asbE) are shown in figures 2-4 and tables S3-S8 (supplementary material). For all three primers the number of gene copies for the free-living portion of the bacterial producers maximized on Oct. 2nd (bloom initiation). For the particle-associated bacteria a different pattern was observed for each of the producers. Thus gene copies of the *Marinobacter* vibrioferrin producers (pvsB primer) showed maxima on Oct. 2nd, Oct. 9th and Oct. 30th and a minimum near the bloom maximum on Oct. 5th, while non-*Marinobacter* producers of vibrioferrin (vibX primer) peaked

on Oct. 2nd and generally declined thereafter. Gene copies of *asbE* from petrobactin producers were more or less constant throughout the study period with a maximum at the end. Overall, gene copy numbers from non-*Marinobacter* vibrioferrin producers constituted the majority of the photoactive siderophore genes detected (ca. 10^9 copies/L) with the *Marinobacter* vibrioferrin producers approximately an order of magnitude less abundant (10^8 copies/L) and the petrobactin producers a small minority (10^6 copies/L). Unfortunately the primers for the gene *iucC* (aerobactin biosynthesis) performed poorly and *iucC* gene copy numbers were below our detection limit at all time points.

Normalizing the gene copy numbers to total bacteria provides an alternate way to look at the data (figure 5). Here, we see that *Marinobacter* and non-*Marinobacter* producers of vibrioferrin constitute the largest percentage of total bacteria (sum of free living and particle-associated bacteria) throughout the time points. Comparison of the total photoactive siderophore producers as a percentage of the total bacteria shows they generally track *L. polyedrum* numbers and maximize at ca. 8.6% of the total bacterial population on October 5th, a date near the bloom maximum.

Phylogeny. Although qPCR requires the use of rather small amplicons (in our case ca. 100-150 bp) which are not ideal for phylogeny studies, as generally speaking the larger the sequences being compared the more accurate the description of diversity, it is still possible to get preliminary data on the community structure of photoactive siderophore producers as a function of bloom dynamics. This data was obtained from clone libraries prepared from our qPCR products. A phylogenetic tree was then constructed from 38 sequences of *asbEII* related clones and 56 sequences of *vibXII* related clones. As seen in figure 6, many of *asbEII* related sequences are clustered together whereas the group of *asbEII* and *vibXII* are rooted at a further point. The

phylogenetic tree was consistent with a common ancestor for most of the sequences related to *asbEII* clones. Similarly, the tree showed a common ancestor among the sequences obtained from *vibXII*. The two groups' *asbEII* and *vibXII* were further rooted indicating that the two groups evolved at a later time than the sequences among the groups. In the course of evolution, the protein sequences from two species that have an ancestor in common may have diverged in a variety of ways such as insertions and deletions of amino acids. The sequences often evolve to adapt to a specific environment.

The clone library was constructed from the randomly selected sequences from *asbEII* and *vibXII* clones representing three environmental groups or communities i.e. beginning, middle, end of bloom. Each community was statistically analyzed by UniFrac software for similarity and difference from other communities.[35,36] Both environment distance matrix analysis and significance analysis concluded that the community of free-living bacteria from beginning time point was significantly different ($p<0.04$) from all the other communities (either free-living or particle-associated) found at later time points (figures S1 and S2, supplementary material). The cluster environment, Principal Coordinates Analysis, PCA (figure 7 and figure S4 supplementary material) and Jackknife environment analyses all supported this result.

Discussion

Using qPCR, we have successfully quantified the biosynthetic genes for the presence of two photoactive siderophores using primers *pvsB* for *Marinobacter* producers of vibrioferrin, *vibXII* for *non-Marinobacter* producers of vibrioferrin, *and asbEII for* petrobactin in the sea surface water during a dinoflagellate bloom at Scripps Pier. The results showed a co-relation of dinoflagellate abundance and the total photoactive siderophore producers expressed as a function of total bacterial numbers. All three groups of siderophore producers reached their peak as a

percentage of the total bacterial numbers on October 5th at or near the bloom maximum. The *non-Marinobacter* producers of vibrioferrin were by far the most abundant at all time points. More specifically, the relative presence of *pvsB, vibXII,* and *asbEII* to the total bacteria during the time points was between 0.2%-0.4%, 0.3%-8.6%, and 0.002%-0.012%, respectively.

Of particular significance is the predominance of producers of the photoactive siderophore vibrioferrin (VF) throughout the bloom which reached a percentage as high as almost 10% of the total bacterial numbers. In contrast, in a previous study of open ocean sites in the North Atlantic we found that petrobactin producers were dominant.[22] Vibrioferrin is unique among photoactive siderophores in that its photoproduct cannot rebind the released Fe(II).[21,37] In contrast, the photoproducts formed from the photolysis for all the other photoactive siderophores studied thus far including petrobactin and aerobactin have been found to retain the ability to coordinate Fe(III) so that the overall photolysis reaction is actually that shown below.[18-20,38]

$$\text{Fe(III)-Sid} + h\nu \rightarrow \text{Sid*} + \text{Fe(II)} \qquad (1)$$

$$\text{Sid*} + \text{Fe(II)} + O_2 \rightarrow \text{Fe(III)-Sid*} \qquad (2)$$

Indeed in some cases the photoproduct (sid*) is actually a *better* Fe(III) chelator than the parent siderophore.[20,38] It has also been shown in the one case where it was studied that the Fe(III) complex of the photoproduct is recognized by the bacteria that produce the parent siderophore and is taken up via the same transport system with equal affinity.[20] This observation throws doubt on the ability of these siderophores to provide a bioavailable source of iron to phytoplankton since strong iron binding ability is retained even after photolysis.

FeVF on the other hand not only undergoes photolysis at a faster rate under relatively low illumination conditions compared to other photoactive siderophores, the resulting photoproduct has *no* significant affinity for Fe(III).[21] Thus the photolysis of Fe(III)-VF is an irreversible

process that leads to the destruction of the siderophore with the complete release of all of the iron as Fe(II). The latter is likely rapidly oxidized by molecular oxygen ultimately yielding a mixture of soluble and insoluble forms of Fe(III) as in equations 3 and 4

$$\text{Fe(III)-VF} + h\nu \rightarrow \text{VF*} + \text{Fe(II)} \qquad (3)$$

$$\text{Fe(II)} + O_2 \rightarrow \text{Fe(III)'} \rightarrow \text{Fe(III)}\downarrow \qquad (4)$$

where Fe(III)' represents transiently soluble iron hydroxo species and Fe(III)↓ represents the increasingly insoluble mineral phases present at equilibrium. This means in practice that under surface illumination conditions bacteria producing VF will see that siderophore rapidly degraded by sunlight with the result of increasing the bioavailability of iron to other organisms including phytoplankton through the formation of soluble Fe(II) and Fe(III)'. Thus with near 9% of the total bacterial population potentially producing VF, large amounts of iron could be constantly recycled into bioavailable forms suitable for supporting phytoplankton growth during the bloom. It is well established through meso-scale iron fertilization experiments that increased bioavailability of iron can lead to large phytoplankton blooms.[39-41]

Finally, analysis of the community structure of petrobactin and non-Marinobacter vibrioferrin producers as a function of bloom dynamics yielded the result that the community of free-living bacteria from the beginning time point was significantly different ($p<0.04$) from the other communities. This observation suggests a distinct community of free living photoactive siderophore producers exists whose production of bioavailable iron via photolysis may be involved in bloom initiation. Subsequently a different, and largely particle associated, community thrives during the bloom maximum and decline. Perhaps this community represents a mutualistic iron for carbon arrangement as recently proposed.[22] Clearly further detailed studies will be needed to further address this hypothesis.

Conclusions

We studied the correlation between the presence of bacteria producing one of four photoactive siderophores relative to total bacterial and dinoflagellate numbers from local surface water at the Scripps Pier before, during, and after summer bloom of the dinoflagellate *L. polyedrum*. The following are the conclusions obtained from this study.

- Using biochemical techniques such as qPCR to quantify the genes encoding for photoactive siderophore biosynthesis in marine bacteria has great potential to serve as surrogates for the presence of such siderophores in the marine environment.
- Photoactive siderophore producing bacteria are relatively abundant representing 1-9% of the total bacterial population and thus they have the potential to alter the bioavailability of iron in marine environments.
- Vibrioferrin, a uniquely photoreactive siderophore, was by far the most abundant photoactive siderophore produced at all time points.
- The community of photoactive siderophores produced by free living bacteria just prior to the dinoflagellate bloom was significantly different than those found during bloom maximum and decline. This suggests that they could be providing a source of bioavailable iron, which in turn could be involved in dinoflagellate bloom initiation.

We hope these findings will aid us in gauging the importance of photoactive siderophores in the marine environment in general and harmful algal bloom dynamics in particular.

Acknowledgements

This work was funded by NOAA Grants #NA04OAR4170038 and NA08OAR4170669, California Sea Grant College Program Project numbers R/CZ-198 and R/CONT-205 and NSF grant CHE-0924313 to CJC. The Southern California Coastal Ocean Observing System, Harmful

Algal Bloom Monitoring Program (MLC and MH) was funded through NOAA Grant # NA11NOS0120029.

References

1. A. J. Lewitus, R. A. Horner, D. A. Caron, E. Garcia-Mendoza, B. M. Hickey, M. Hunter, D. D. Huppert, R. M. Kudela, G. W. Langlois, J. L. Largier, E. J. Lessard, R. RaLonde, J. E. J. Rensel, P. G. Strutton, V. L. Trainer, and J. F. Tweddle, *Harmful Algae*, 2012,**19**, 133.
2. H. J. Kim, A. J. Miller, J. McGowan and M. L. Carter, *Progress in Oceanography*, 2009, **82**, 137.
3. D. M. Anderson, A. D. Cembella, and G. M. Hallegraeff, *Annual Review in Marine Science*, 2012, **4**, 143.
4. S. Honner, K. M. Kudela, and E. Handler, *Journal of Emergency Medicine*, 2010, **43**, 663.
5. F. Azam and A. Z. Worden, *Science*, 2004, **303,** 1622.
6. F. Azam and F. Malfatti, *Nat. Rev. Microbiol.*, 2007, **5**, 782.
7. J. N. Rooney-Varga, M. W. Giewat, M. C. Savin, S. Sood, M. LeGresley, and J. L. Martin, *Microb. Ecol.*, 2005, **49**, 163.
8. X. Mayali and F. Azam, *J. Eukaryot. Microbiol.*, 2004, **51**, 139.
9. X. Mayali, P. J. S. Franks, Y. Tanaka, and F. Azam, *Journal of Phycology*, 2008, **44**, 923.
10. C.J.S. Bolch, T. Subramanian and D.H. Green, 2011, *Journal of Phycology*, 2011, **47**, 1009.
11. D. H. Green, L. E. Llewellyn, A. P. Negri, S. I. Blackburn, and C. J. S. Bolch, *FEMS Microbiology Ecology*, 2004, **47**, 345.
12. K. W. Bruland, J. R. Donat, and D. A. Hutchins, *Limnology and Oceanography*, 1991, **36**, 1555.
13. J. H. Martin and S. E. Fitzwater, *Nature*, 1988, **331**, 341.
14. J. F. Wu and G. W. Luther, *Limnology and Oceanography*, 1994, **39**, 1119.
15. M. Sandy and A. Butler, *Chem Rev*., 2009, **109**, 4580.

16. P. D. Tortell, M. T. Maldonado and N. M. Price, *Nature*, 1996, **383**, 330.

17. J. M. Vraspir and A. Butler, *Annu. Rev. Mar. Sci.*, 2009, **1**, 43.

18. K. Barbeau, E. L. Bruland, A. Butler, *Nature*, 2001, **413**, 409.

19. K. Barbeau, G. P. Zhang, D. H. Live and A. Butler, *Journal of the American Chemical Society*, 2002, **124**, 378.

20. F. C. Küpper, C. J. Carrano, J. U. Kuhn and A. Butler, *Inorg. Chem.*, 2006, **45**, 6028.

21. S. A. Amin, D. H. Green, M. C. Hart, F. C. Küpper, W. G. Sunda, and C. J. Carrano, *Proc Natl Acad Sci USA*, 2009, **106**, 17071.

22. A. Gärdes, C. Triana, S. A. Amin, D. H. Green, L. Trimble, A. Romano, and C. J. Carrano, *BioMetals*, 2013, **26**, 507.

23. V. Tai, and B. Palenik, *ISME J*., 2009, **8**, 903.

24. E. L. Venrick and T. L. Hayward, *CalCOFI Report*, 1984, **25,** 74.

25. Uthermöl, *Mitteilungen-Internationale Vereinigung für Theoretische und Angewandte Limnologie*, 1958, **9,** 1.

26. A. Sournia, *Phytoplankton Manual*, 1978, 191-196.

27. D. Tillett and B. A. Neilan, *Journal of Phycology*, 2000, **36,** 251.

28. M. Yilmaz and E. J. Phlips, *Journal of Phycology*, 2009, **45,** 517.

29. H. J. Bach, J. Tomanova, M. Schloter, J. C. Munch, *Journal of Microbiological Methods*, 2002, **49,** 235.

30. (a) M. Labrenz, I. Brettar, R. Christen, S. Flavier, J. Botel, M. G. Hofle, Appl. Envir. Micro., 2004, 70, 4971. (b) H. J. Bach, J. Tomanova, M. Schloter, J. C. Munch, *J. Microbiol. Methods*, 2002, **49**, 235.

31. J. Raes, J. O. Korbel, M. J. Lercher, C. von Mering and P. Bork, *Genome Biology*, 2007, **8**,

R10.

32. E. Bier, S. Sun and E. C. Howard, Appl. *Envir. Micro.*, 2009, **75**, 2221.

33. K. Katoh, K. Misawa, K. Kuma and T. Miyata, *Nucleic Acids Res.*, 2002, **30,** 3059.

34. S. Guindon and O. Gascuel, *Syst Biol*., 2003, **52,** 696.

35. C. Lozupone and R. Knight, *Appl Environ Microb.*, 2005, **71**, 8228.

36. C. Lozupone, M. Hamady, and R. Knight, *Bmc. Bioinformatics*, 2006, 7.

37. S. A. Amin, D. H. Green, F. C. Küpper, C. J. Carrano, *Inorg. Chem.*, 2009, **48**, 11451.

38. R. J. Abergel, A. M. Zawadzka and K. N. Raymond, *J Am Chem Soc.*, 2008, **130**, 2124.

39. E. L. Rue and K. W. Bruland, *Limnology and Oceanography*, 1997, **42**, 901.

40. P. W. Boyd, A. J. Watson, C. S. Law, E. R. Abraham, T. Trull, *Nature*, 2000, 407, **695**.

41. K. H. Coale, K. S. Johnson, S. E. Fitzwater, R. M. Gordon, S. Tanner, *Nature*, 1996, **383**, 495.

Figure 1.

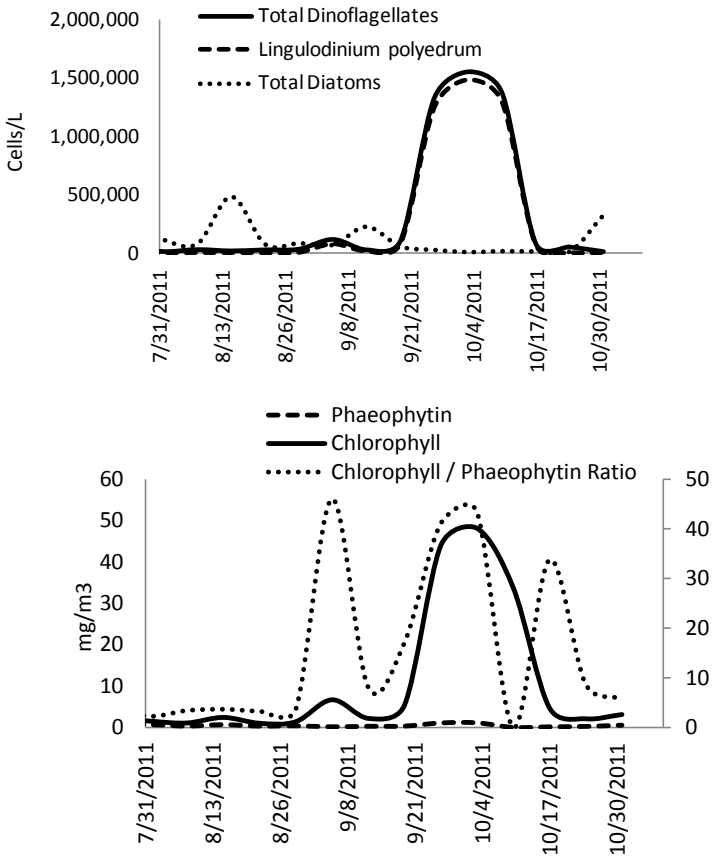

Figure 2.

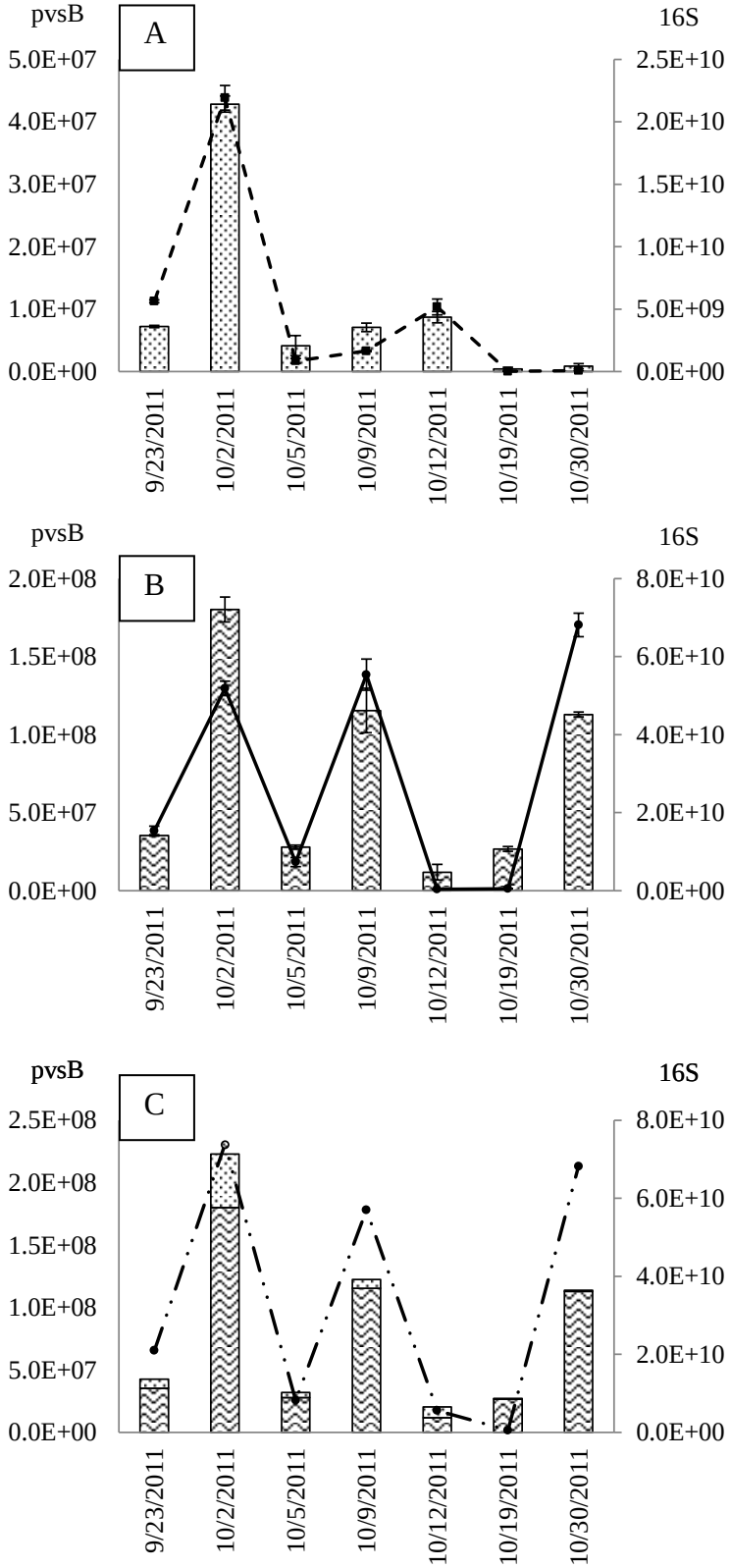

Figure 3.

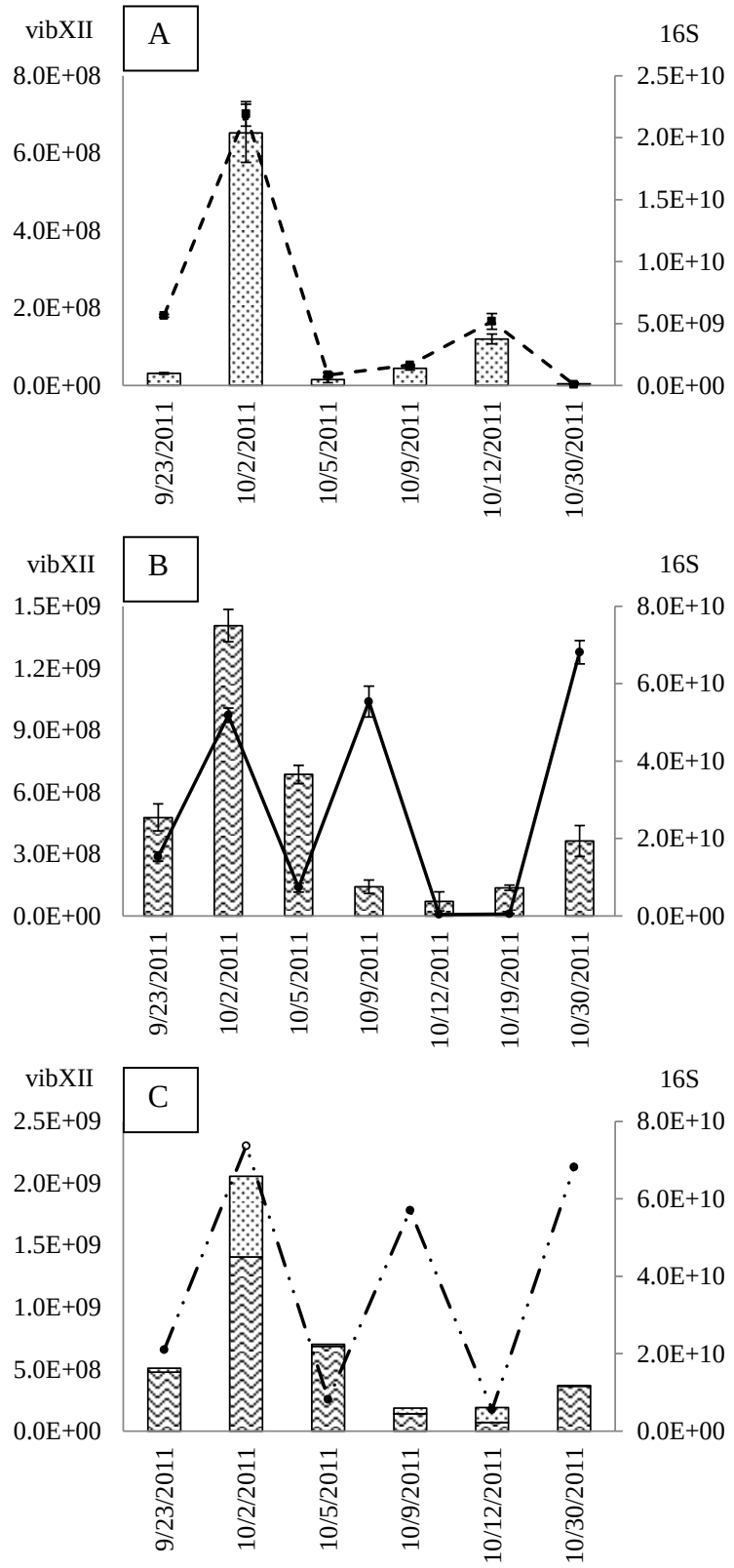

Figure 4.

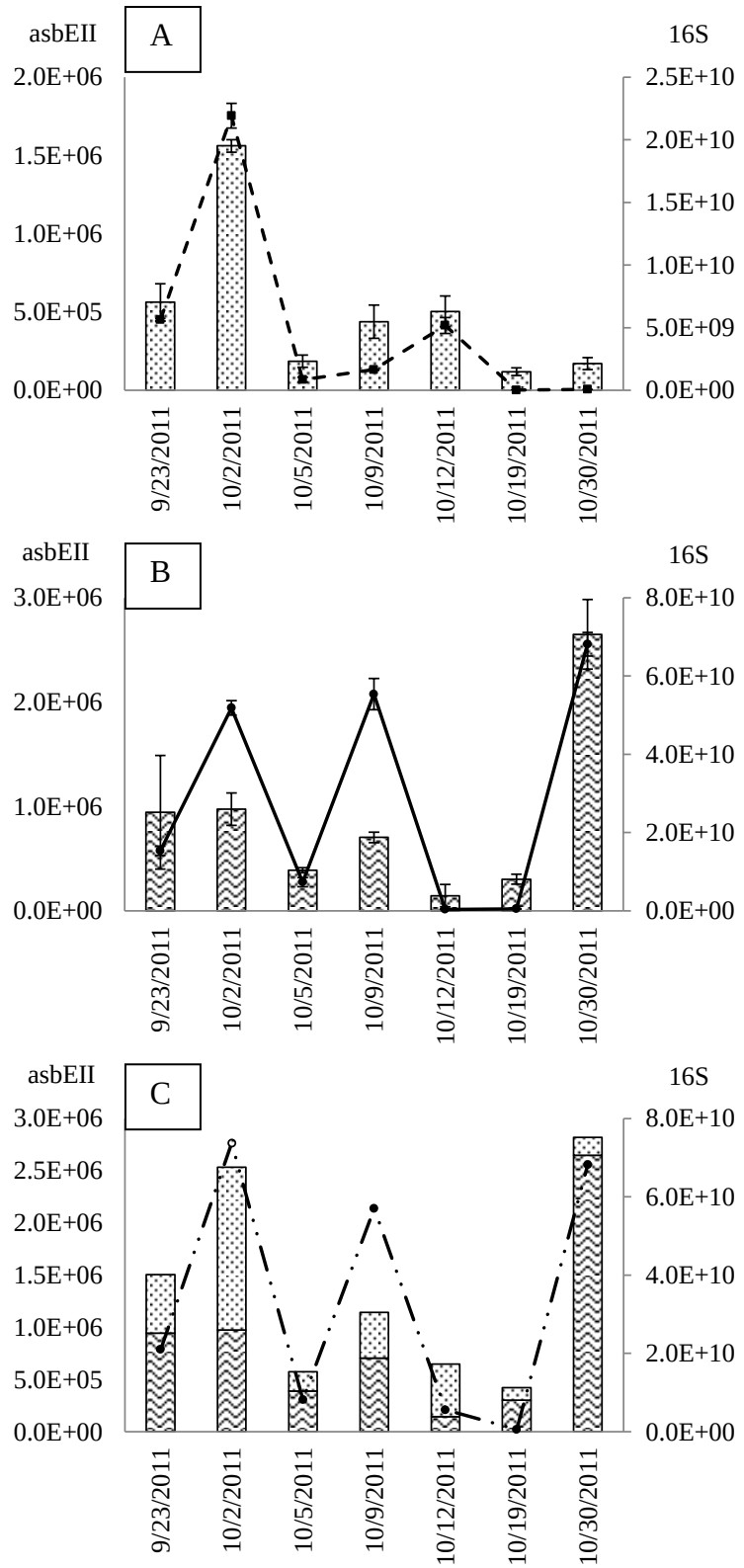

Figure 5.

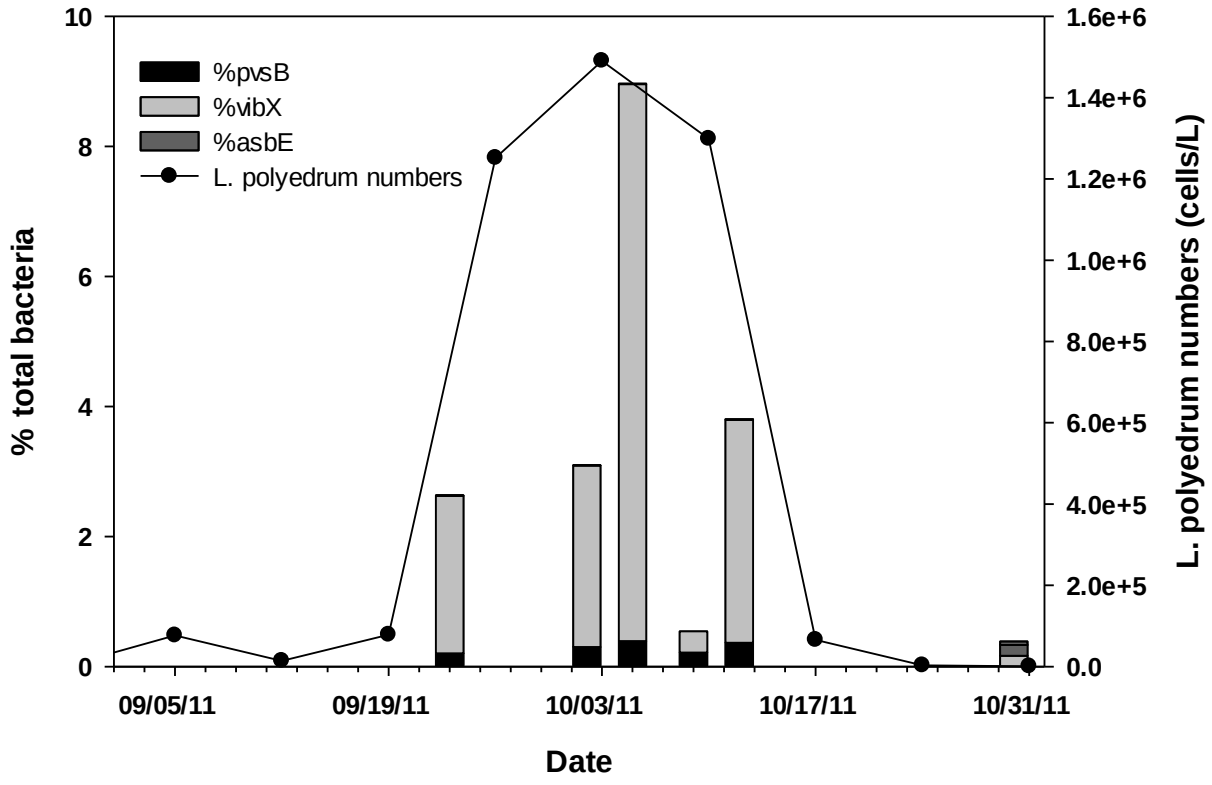

Figure 6.

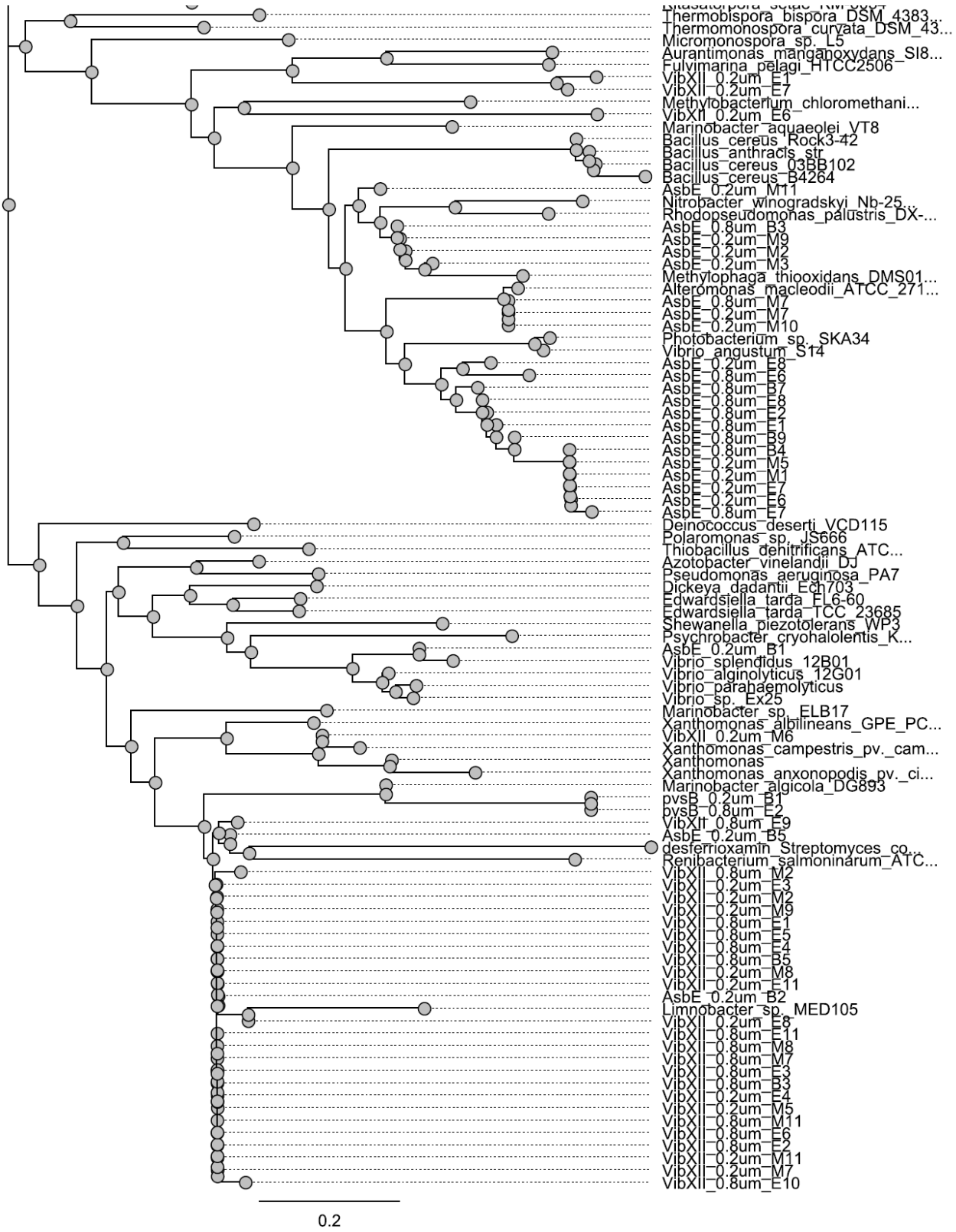

Figure 7.

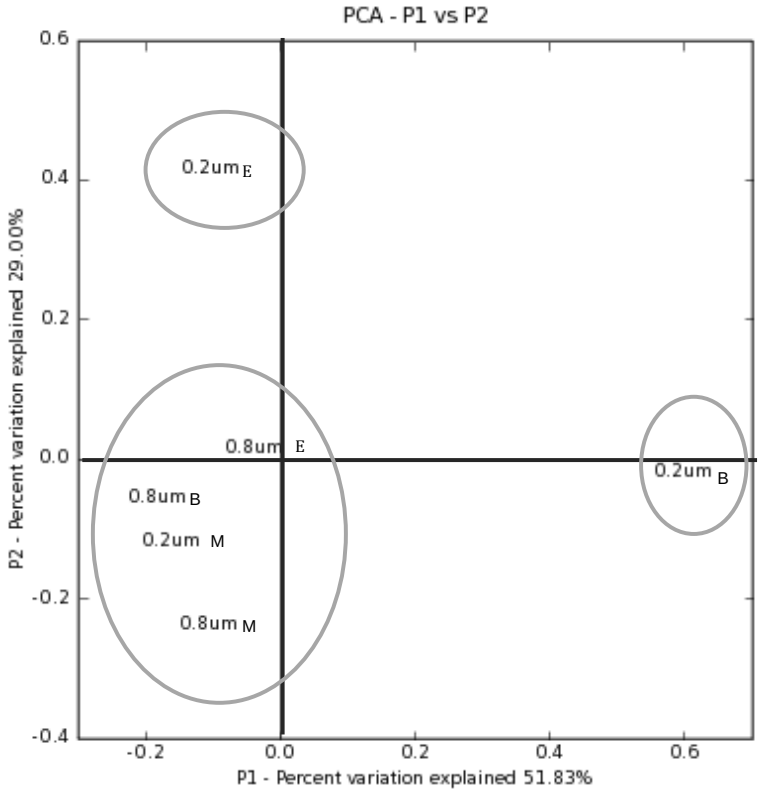

Figure Captions

Figure 1. Upper panel: Cell numbers *L. polyedrum*, total dinoflagellates, and diatoms by date. Lower panel: Chlorophyll, Phaeophytin and the Chlorophyll/Phaeophytin ratio (mg/m^3) by date.

Figure 2. A) Bar graph shows free-living *Marinobacter* (0.2μm fraction) derived *pvsB* gene copy numbers. Dotted line represents free-living bacterial numbers (16S gene copy number from 0.2μm fraction) B) Bar graph shows particle-associated *Marinobacter* (0.8μm fraction) derived *pvsB* gene copy number. Solid line represents particle-associated bacterial numbers (16S gene copy number from 0.8μm fraction). Error bars are the average ± one standard deviation of triplicate measurements. C) Total *pvsB* gene copy number and total 16S gene copy number (dot-dash) are shown.

Figure 3. A) Bar graph shows free-living non-*Marinobacter* (0.2μm fraction) derived *pvsB* gene copy numbers. Dotted line represents free-living bacterial numbers (16S gene copy number from 0.2μm fraction) B) Bar graph shows particle-associated non-*Marinobacter* (0.8μm fraction) derived *pvsB* gene copy number. Solid line represents particle-associated bacterial numbers (16S gene copy number from 0.8μm fraction). Error bars are the average ± one standard deviation of triplicate measurements. C) Total *pvsB* gene copy number and total 16S gene copy number (dot-dash) are shown.

Figure 4. A) Bar graph shows free-living (0.2μm fraction) derived *asbEII* gene copy numbers. Dotted line represents free-living bacterial numbers (16S gene copy number from 0.2μm

fraction) B) Bar graph shows particle-associated (0.8μm fraction) derived *asbEII* gene copy number. Solid line represents particle-associated bacterial numbers (16S gene copy number from 0.8μm fraction). Error bars are the average ± one standard deviation of triplicate measurements. C) Total *pvsB* gene copy number and total 16S gene copy number (dot-dash) are shown.

Figure 5. Bar graph shows the percentage of total siderophore genes i.e. *pvsB* (both *Marinoacter* and non-*Marinobacter* derived) and *asbEII* relative to the total 16S gene copy number. Line shows *L. polyedrum* numbers.

Figure 6. Phylogenetic Tree derived from clones obtained by *vibXII* and *asbEII* primers. The protein sequences were uploaded to Geneious R6. The phylogenetc tree of *asbEII* and *vibXII* was constructed from 38 sequences and 56 sequences which included both samples and references.

Figure 7. Principal Coordinates Analysis (PCA). The first principal component (the X-axis) separates the free-living community from beginning of the Red tide from other communities. The second principal component (the Y-axis) separates the free-living community from end of the Red tide from other communities although based on the Unifrac analysis only the former is statistically significant ($p<0.04$).